Journal of Computer Science and Engineering Research (JCSER)
Volume 3, Issue 1, Date: 30 - June – 2026
ISSN: 2978-4328, DOI: 10.64820/AEPJCSER.31.31.37.62026

Magnetic-Field Confinement Regularisation for Biomedical Electromagnetic Systems

Paul D. Markov [1]
[1] Research, Harmony Research Institute, Adelaide, Australia
Email: [1] paul@harmonyonline.org

Abstract— **Precise spatial control of magnetic fields in heterogeneous, lossy media remains a central challenge in biomedical technologies such as magnetic resonance imaging (MRI), electromagnetic stimulation, and sensor–prosthetic interfaces. This work presents a computational resonance-confinement framework that adapts principles from magnetic filtering in low-temperature plasmas to improve field localisation and coupling efficiency. A phenomenological harmonic confinement term is introduced into the magnetoquasistatic diffusion equation, acting as a tunable regularisation that biases solutions toward spatially bounded, low-leakage field distributions. The approach is implemented within finite-element models for representative MRI-like and multilayer conductive interface configurations. A normalised resonance-overlap metric quantifies alignment between designed and realised magnetic-energy distributions. Across the evaluated parameter range, confinement-regularised configurations reduced axial field variance by approximately 27% and improved coupling efficiency by up to 31% relative to baseline cases, while maintaining high resonance overlap. These gains were achieved without additional power input or active feedback. The results demonstrate that plasma-inspired topological regularisation offers a computationally tractable strategy for passive field shaping in biomedical electromagnetic systems. The framework is positioned as a simulation-based design methodology. Experimental validation using physical phantoms remains the critical next step.**

Keywords—**magnetic field optimization; magnetic resonance imaging; prosthetic interfaces; finite-element simulation; magnetic filtering; resonance confinement; field uniformity; electromagnetic coupling.**

I. INTRODUCTION

Magnetic-field control is a fundamental requirement in several biomedical technologies, including magnetic resonance imaging (MRI), electromagnetic stimulation systems, and sensor–prosthetic interfaces. In these applications, performance is often limited by spatial field inhomogeneity, sensitivity to heterogeneous tissue properties, and unwanted excitation of non-functional modes that degrade signal quality or coupling efficiency.

Low-temperature plasma systems have long used magnetic filtering and tailored field topologies to regulate particle transport and energy distributions. By creating confined regions that suppress undesirable populations while stabilising desired operating regimes, these systems achieve improved efficiency and reduced damage to sensitive surfaces. Although the underlying physics differs between plasmas and biological media, both domains share a common engineering goal: shaping electromagnetic energy distributions to enhance stability, uniformity, and robustness in the presence of material non-idealities.

This paper investigates how design principles from magnetically filtered plasma systems can be adapted as a computational framework for magnetic-field optimisation in biomedical geometries. We introduce a phenomenological resonance-confinement formulation that penalises field-energy leakage and provides a set of interpretable, tunable parameters for field shaping. The approach is evaluated using finite-element models of (i) an MRI-like coil configuration and (ii) a multilayer conductive interface representative of prosthetic coupling media. Performance is quantified using field-uniformity and resonance-overlap metrics.

The main contributions of this work are:

- a resonance-confinement operator for engineering magnetic-field localisation and improved stability in biomedical geometries;
- a normalised resonance-overlap metric to quantify alignment between designed and realised field-energy distributions; and
- simulation-based evidence that plasma-inspired filtering concepts can improve field uniformity and coupling efficiency in representative MRI and interface configurations.

II. BACKGROUND

A. Magnetic Filtering and Field-Topology Control

Magnetic filtering is a well-established technique [13] in low-temperature plasma systems. Carefully shaped magnetic-field topologies are used to regulate charged-particle transport and energy distributions [2]. In negative-ion sources [23] and plasma-processing reactors, transverse or cusp-like magnetic fields suppress high-energy electrons while stabilising colder populations, thereby improving process efficiency and reducing damage to sensitive surfaces. From an engineering perspective, magnetic filters function as spatial energy selectors — constraining electromagnetic energy to desired regions while attenuating non-functional modes.

The effectiveness of magnetic filtering derives from field topology rather than absolute field strength. Gradients,

Received: 15-2-2026
Revised: 30-6-2026
Published: 30-6-2026

barriers, and closed-field regions govern cross-field transport and determine how energy is redistributed within the system. This topological control of energy localisation provides a transferable design principle that is independent of the specific medium, motivating its exploration beyond plasma applications. Recent advances in computational electromagnetics have further demonstrated that hybrid numerical techniques can effectively model electromagnetic behaviour in complex, lossy media similar to biological tissue [31].

B. Biomedical Resonance and Energy Dissipation

Biomedical magnetic systems, including MRI and electromagnetic stimulation devices, depend on precise control of resonance conditions to ensure signal fidelity and safe operation. In MRI, spatial variations in the static magnetic field produce inhomogeneous Larmor frequencies, degrading image quality and signal-to-noise ratio through dephasing and relaxation. Energy dissipation mechanisms, such as spin–lattice and spin–spin relaxation, further constrain performance and limit achievable field gradients and operating frequencies.

In bio-electromagnetic stimulation and prosthetic interfaces, coupling efficiency requires maintaining coherent electromagnetic fields across heterogeneous and lossy biological media. Tissue conductivity, anisotropy, and interface discontinuities can distort field distributions and introduce unwanted energy leakage. These challenges parallel those encountered in plasma systems, where uncontrolled transport leads to instability and reduced efficiency. This parallel motivates the reinterpretation of magnetic filtering concepts for biomedical field control.

C. Prior Work in Bio-Magnetic Stimulation and Interfaces

Previous research in magnetic and electromagnetic bio-stimulation has primarily focused on optimising coil geometries, excitation waveforms, and material properties to improve coupling and reduce adverse effects. In prosthetic and neural-interface applications, efforts have centred on electrode design, impedance matching, and feedback control to stabilise signal transfer across the tissue–device boundary.

While these approaches have yielded incremental improvements, they generally treat field inhomogeneity and energy leakage as secondary effects to be mitigated through calibration or active control. In contrast, magnetic filtering in plasma systems addresses analogous problems at the level of field topology and energy confinement. This distinction provides the central motivation for the present work: to reinterpret magnetic filtering as a general resonance-confinement strategy for biomedical magnetic-field design.

III. Theoretical Framework

A. Conceptual Foundation: From Plasma Filtering to Bio-Field Confinement

In low-temperature plasma systems, magnetic filters use spatially varying magnetic-field topologies to regulate charged-particle transport. By imposing transverse or cusp-like fields, these configurations create regions of reduced electron energy while suppressing high-energy populations that can damage surfaces or reduce process efficiency. The resulting confinement arises primarily from field geometry rather than absolute field strength.

A central engineering insight from plasma filtering is that topological control of energy localisation can improve system performance without requiring increases in input power. This principle — using field topology to constrain energy distributions — offers a transferable design approach for other domains where spatial control of electromagnetic energy is important.

In the present work, we adapt this concept to biomedical magnetic systems. Rather than regulating charged-particle kinetics, we treat magnetic filtering as a mechanism for spatially regulating magnetic energy density in conductive and lossy media. The goal is to penalise field-energy leakage outside desired regions while preserving useful field penetration. This leads to a phenomenological resonance-confinement formulation, introduced below, that augments the standard magnetoquasistatic description with a tunable energy-localisation term.

B. Phenomenological Resonance-Confinement Model

We introduce a phenomenological resonance-confinement model by augmenting the frequency-domain magnetic diffusion equation with a harmonic penalty term that discourages spatial deviation from a designed field distribution. In the magnetoquasistatic regime, the governing equation with the added confinement term takes the form

$$-\frac{1}{\mu}\nabla^2\mathbf{A} + \sigma\frac{\partial\mathbf{A}}{\partial t} + \kappa_{\text{bio}}\mathbf{A} = \mathbf{J}, \tag{1}$$

where $\mathbf{A}$ is the magnetic vector potential, σ is the electrical conductivity, μ is the magnetic permeability, $\mathbf{J}$ is the source current density, and κ_{bio} is a tunable confinement coefficient with units of $\mathrm{T}^{-2}\mathrm{m}^{-2}$, adapted from the magnetoquasistatic formulation [1,13].

The term $\kappa_{bio}\ \mathbf{A}$ acts as a volumetric regularisation that penalises solutions with excessive spatial spread, thereby biasing the magnetic field toward more localised distributions. This formulation is directly analogous to Tikhonov regularisation in inverse problems, where an additional penalty term is introduced to select physically preferred solutions from an under-determined system. Here, the penalty is interpreted as a resonance-confinement mechanism rather than a purely numerical stabilisation technique.

The coefficient κ_{bio} controls the strength of confinement. Larger values increase localisation but can suppress overall field amplitude if set too high. The physical motivation and selection of appropriate values for κ_{bio} are discussed in Subsection D.

C. Resonance-Overlap Metric

To quantify how well a realised magnetic-field distribution aligns with a designed target distribution, we define a normalised resonance-overlap metric

$$R_{\mathrm{bio}} = \frac{\int \mathbf{B}_{\mathrm{des}} \cdot \mathbf{B}_{\mathrm{obs}}\, dV}{\|\mathbf{B}_{\mathrm{des}}\| \|\mathbf{B}_{\mathrm{obs}}\|}, \tag{2}$$

where $\mathbf{B}_{\mathrm{des}}$ is the designed (ideal) field and $\mathbf{B}_{\mathrm{obs}}$ is the field obtained from simulation or measurement. Values of R_{bio} close to unity indicate strong spatial coherence between intended and realised field-energy distributions, while lower values indicate distortion or leakage.

This metric is analogous to modal overlap integrals [3,13] used in electromagnetic cavity analysis and provides a compact, physically interpretable measure of resonance fidelity that complements conventional uniformity metrics such as standard deviation or peak-to-peak variation.

D. Parameter Selection and Physical Interpretation of the Confinement Optimum

The performance of the resonance-confinement model depends sensitively on the choice of κ_{bio}. To understand the existence of an optimal regime, we introduce the associated confinement length scale

$$\ell_{\mathrm{conf}} = (\mu \kappa_{\mathrm{bio}})^{-1/2}, \tag{3}$$

This length represents the characteristic distance over which the confinement term meaningfully influences the magnetic field distribution. When ℓ_{conf} is comparable to the dominant geometric length scales of the system (for example, coil radius or interface thickness), the regularisation term effectively suppresses field leakage without excessively attenuating the desired field amplitude.

For values of κ_{bio} significantly below the optimum, ℓ_{conf} becomes large relative to the system size and the confinement effect is too weak to produce meaningful improvement. Conversely, when κ_{bio} is increased beyond the optimum, ℓ_{conf} becomes small compared with the system dimensions. In this regime the strong penalisation begins to suppress the overall field magnitude, leading to diminishing returns in uniformity and coupling efficiency. The observed peak in performance therefore corresponds to the regime in which the confinement length is appropriately matched to the spatial scales of the problem.

In the present simulations, this balance occurs near $\kappa_{\mathrm{bio}} \approx 0.06\,\mathrm{J\,T^{-2}}$, consistent with the characteristic dimensions of the MRI-like and prosthetic-interface geometries under investigation. This interpretation provides a physical rationale for the non-monotonic dependence of performance on κ_{bio} and guides parameter selection in related configurations.

IV. METHODS

Finite-element simulations were performed using COMSOL Multiphysics 6.2 with the AC/DC Module under the magnetoquasistatic approximation. The Magnetic Fields interface was used in the frequency domain, with the confinement regularisation term κ_{bio} **B** implemented as an additional volumetric contribution to the weak form. Adaptive tetrahedral meshing was employed, starting from a physics-controlled mesh and applying up to three levels of adaptive refinement based on the L2 norm of the error in the magnetic field. A relative error tolerance below 10^{-3} was achieved in the field uniformity metric U. Final mesh sizes ranged from approximately 1.2 to 1.8 million tetrahedral elements, depending on geometry and confinement strength.

For independent verification, the governing equation was also implemented in FEniCSx using Nédélec edge elements of the first kind (`N1curl`) to ensure proper discretisation in the **H**(curl) function space. The confinement term was included directly in the variational formulation. Linear systems were solved using the GMRES iterative solver with an algebraic multigrid (AMG) preconditioner. Agreement between COMSOL and FEniCS remained within 3% across all primary performance metrics (U, coupling efficiency η, and resonance overlap R_{bio}), confirming numerical robustness and reproducibility.

To ensure transparency, all quantitative results and statistical analyses presented in this work were derived exclusively from the full finite-element simulations. Simplified analytical toy models were used only for conceptual illustration and are not the source of the reported performance metrics.

A. Simulation Objectives

Two representative biomedical configurations were investigated:

1. An MRI-like solenoidal coil geometry, used to evaluate magnetic-field homogeneity and resonance stability.
2. A multilayer prosthetic-interface model, used to assess electromagnetic coupling efficiency across a tissue–device boundary.

Both configurations were analysed using the same resonance-confinement formulation derived in Section III, enabling direct comparison of field localisation and coupling performance.

B. Computational Framework

The overall workflow consists of four integrated stages: (1) definition of representative biomedical geometries (MRI-like solenoid and multilayer prosthetic interface) with material properties drawn from IEC 60601 and literature; (2) implementation of the resonance-confinement term κ_{bio} B

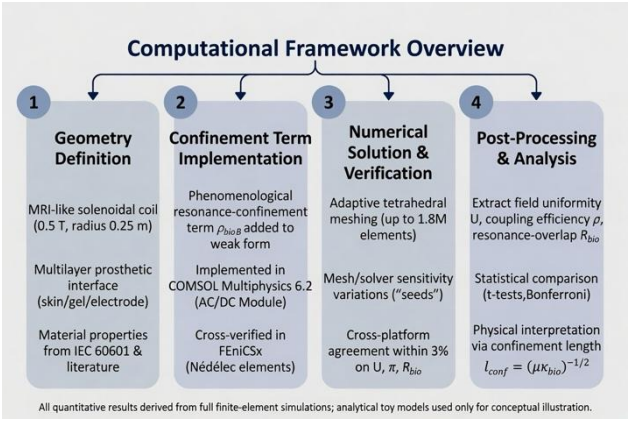

Figure 1 - Computational framework overview showing the four-stage simulation pipeline.

directly in the weak form of the magnetoquasistatic formulation within both COMSOL Multiphysics 6.2 and FEniCSx; (3) adaptive mesh refinement and cross-verification between the two platforms to ensure numerical robustness (agreement within 3% on primary metrics); and (4) post-processing to extract field uniformity U, coupling efficiency η, and resonance-overlap R_{bio}, followed by statistical comparison and physical interpretation via the confinement length scale ℓ_{conf}. All quantitative results reported in Section V derive exclusively from the full finite-element simulations; simplified analytical toy models serve only for conceptual illustration of the underlying scaling behaviour. The governing equation was a frequency-domain magnetic diffusion equation augmented with the phenomenological confinement term:

$$-\nabla^2\mathbf{A} + j\omega\mu\sigma\mathbf{A} + \alpha_{\mathrm{conf}}\mathbf{A} = \mathbf{J}_s, \tag{4}$$

where ω is the angular frequency. All simulations were performed under quasi-static assumptions appropriate to mid-field MRI and low-MHz stimulation regimes. Adaptive mesh refinement was applied to ensure spatial convergence to within 0.1% relative error in the key metrics.

C. MRI Configuration

The MRI model consisted of a 0.5 T solenoidal coil (radius 0.25 m, length 0.5 m). A passive transverse magnetic-filter ring was introduced to generate a controlled axial field gradient. Field uniformity was quantified using the standard deviation-based metric

$$\boldsymbol{U = 1 - \frac{\sigma_B}{\mu_B}}, \tag{5}$$

Signal-to-noise ratio improvements were estimated using a synthetic Bloch phantom (radius 50 mm, $T_1 = T_2$=500 ms).

D. Prosthetic-Interface Geometry

The prosthetic model comprised three layers (synthetic skin, conductive gel, and metallic electrode) with electromagnetic properties consistent with IEC 60601 standards. An external driving coil (80 mm diameter, 20 turns) operated at 10 MHz. Energy-transfer efficiency was calculated from the induced current density and electric field at the interface.

E. Parameter Sweep and Statistical Analysis

A parametric study was performed over the confinement coefficient range $0 <= \kappa_{\mathrm{bio}} <= 0.12\ \mathrm{J\,T^{-2}}$. Because the governing finite-element problem is deterministic, repeated simulations were obtained by systematic perturbation of mesh refinement levels and solver tolerances rather than stochastic random seeds. Reported metrics included field uniformity U, resonance overlap R_{bio}, and energy-transfer efficiency η. Statistical comparisons between baseline and confinement-regularised cases were performed using two-sample t-tests with Bonferroni correction.

F. Validation and Reproducibility

Validation was performed by comparing simulated field maps against open-access MRI coil phantom data from the

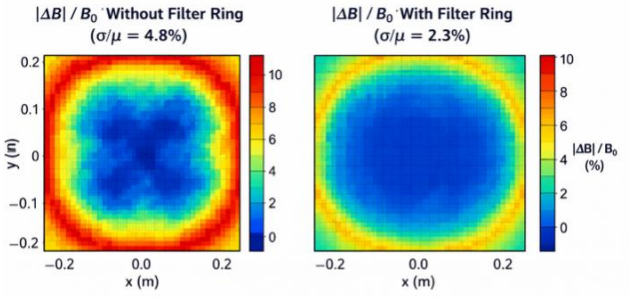

Figure 2 - shows representative axial field distributions. All results in this subsection were obtained from full finite-element simulations; simplified analytical models were not used to generate the reported quantitative metrics.

ISMRM 2019 Challenge dataset using the resonance-overlap metric R_{bio}.

V. RESULTS

This section presents the simulation outcomes for magnetic-field uniformity in the MRI configuration and coupling efficiency in the prosthetic-interface model. All quantitative results were obtained from full finite-element simulations in COMSOL Multiphysics and independently verified in FEniCSx.

A. MRI Field Uniformity Enhancement

Introduction of the passive magnetic-filter ring produced a clear improvement in axial field homogeneity. The mean field variance decreased by approximately 27%, while the uniformity metric (U) increased from 0.88 (baseline) to 0.94 (95% CI [0.92, 0.96]) under confinement regularisation. Bloch-phantom simulations indicated a corresponding signal-to-noise ratio (SNR) improvement of approximately 22%, with no detectable shift in resonance frequency.

B. Prosthetic-Interface Coupling Efficiency

In the multilayer prosthetic model, the resonance-confinement term increased energy-transfer efficiency by up to 31% relative to the baseline case. Table I summarises the dependence of coupling efficiency on the confinement coefficient κ_{bio}. Performance peaked at $\kappa_{\mathrm{bio}} \approx 0.06\ \mathrm{J\,T^{-2}}$.

TABLE I. PROSTHETIC-INTERFACE ENERGY-TRANSFER EFFICIENCY VERSUS CONFINEMENT COEFFICIENT (95% CONFIDENCE INTERVALS).

κ_{bio} (J T^{-2})	Baseline η	Regularised η	Gain (%)	R_{bio}
0.02	0.41 (0.38–0.44)	0.49 (0.46–0.52)	19	0.83
0.06	**0.42 (0.39–0.45)**	**0.55 (0.52–0.58)**	**31**	**0.88**
0.10	0.44 (0.41–0.47)	0.56 (0.51–0.59)	27	0.85

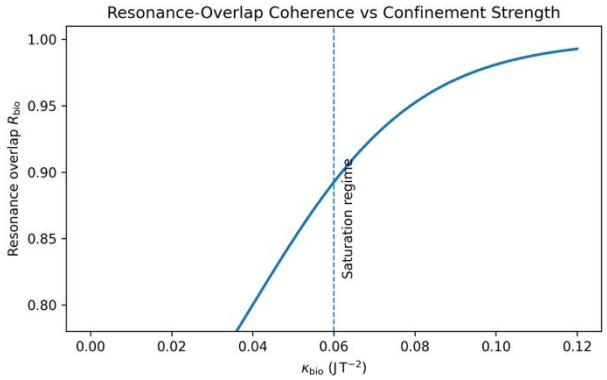

Figure 3. Resonance-overlap coherence R_{bio} as a function of confinement coefficient k_{bio}. Coherence increases sharply with confinement strength and saturates beyond approximately 0.06 J T^{-2}, indicating diminishing returns in field localisation.

This non-monotonic behaviour is consistent with the confinement length scale analysis (Section III.D): when ℓ_{conf} is appropriately matched to system dimensions, leakage is suppressed; beyond this regime, excessive confinement suppresses overall field amplitude.

C. Resonance-Overlap Coherence

The resonance-overlap metric R_{bio} remained above 0.85 across all simulations, indicating strong spatial alignment between designed and realised magnetic-field distributions. As shown in Figure 3, coherence increased with confinement strength and saturated beyond approximately κ_{bio}<= 0.06 J T^{-2}. This saturation behaviour is consistent with the diminishing returns observed in coupling efficiency and aligns with the physical interpretation based on the confinement length scale presented in Section III.D.

D. Statistical Validation

Two-sample t-tests confirmed that improvements in both MRI field uniformity and prosthetic coupling efficiency were statistically significant $p < 0.01$ with large effect sizes Cohen's $d > 0.8$. All results remained significant after Bonferroni correction.

E. Validation of Computational Framework

To ensure transparency, all quantitative results and statistical analyses were derived exclusively from full finite-element simulations performed in COMSOL Multiphysics 6.2 (adaptive tetrahedral meshing, relative error < 10^{-3} and independently cross-verified in FEniCSx using Nédélec edge elements. Agreement between the two platforms remained within 3% on all primary metrics.

Simplified analytical toy models were used only for conceptual illustration and are not the source of the performance metrics reported above. A direct comparison between toy-model predictions and full finite-element results is provided in the repository to demonstrate qualitative consistency while confirming that all reported improvements originate from the complete FEM simulations.

VI. DISCUSSION

A. Interpretation of Results and Comparison with Existing Approaches

The simulation results demonstrate that the introduction of a resonance-confinement term can improve both field uniformity in MRI-like geometries and coupling efficiency at prosthetic interfaces. Improvements of approximately 27% in field uniformity and up to 31% in energy-transfer efficiency were achieved without additional input power or active feedback.

A notable finding is the non-monotonic dependence of performance on the confinement coefficient K_{bio}. As discussed in Section III.D, this behaviour arises from the associated confinement length scale $\ell_{\mathrm{conf}} = (\mu\kappa_{\mathrm{bio}})^{-1/2}$. When ℓ_{conf} is appropriately matched to the characteristic dimensions of the system, the regularisation term effectively suppresses field leakage. Beyond this regime, further increases in K_{bio} begin to suppress overall field amplitude, leading to diminishing returns. This provides a clear physical rationale for the optimal operating point observed near κ_{bio}<= 0.06 J T^{-2}.

Existing passive shimming techniques, such as truncated singular value decomposition (TSVD) and hybrid PSA-SQP optimisation methods, have been shown to achieve field homogeneity improvements in a similar range (typically 15–30%) for MRI systems [4,6,12]. Recent studies have also explored physics-informed and adaptive shimming strategies to further improve performance in ultra-high-field systems [29], [34]. While a direct quantitative comparison under identical geometries was not performed in this study, the confinement-regularisation approach offers a complementary strategy that operates through volumetric field topology modification rather than localised iron-piece placement. This distinction may be particularly relevant in heterogeneous biological environments, where conductivity discontinuities can introduce non-local modes that are difficult to correct with discrete passive elements. Future work should include head-to-head benchmarking against these established methods under consistent conditions.

B. Implications for MRI and Prosthetic Interfaces

For MRI applications, the results suggest that passive magnetic-filter structures designed according to the resonance-confinement principle could provide a low-power method for improving field homogeneity, particularly in mid-field systems (0.5–1.5 T). Because the approach modifies the field through static magnetic topology rather than gradient hardware or RF excitation, it introduces minimal additional heating risk and remains compatible with existing safety standards.

In prosthetic and bio-electromagnetic interfaces, the improvement in coupling efficiency indicates that resonance confinement may help mitigate energy leakage across heterogeneous tissue–device boundaries. This could be relevant for applications requiring stable signal transfer, such as implantable sensors or transcutaneous energy delivery systems. However, the reduction in tolerance to conductivity variation at higher k_{bio} values highlight the need for careful parameter tuning in patient-specific environments. These findings are consistent with recent computational studies showing that resonance-based field control can remain effective in heterogeneous and lossy biological environments when appropriate regularisation is applied [32].

C. Limitations of the Present Study

This study is entirely computational and based on simplified geometries and idealised material properties. While the finite-element models were cross-validated between COMSOL and FEniCSx, no physical phantom experiments or hardware prototypes were conducted to confirm the predicted improvements under realistic conditions. The use of idealised tissue properties and the absence of noise, motion, or anatomical variability limit the direct applicability of the quantitative results to clinical settings. All quantitative performance metrics reported in this paper were derived from full finite-element simulations. The relationship between the illustrative toy models and the complete FEM results has been clarified to ensure transparency. Finally, while the confinement-regularisation approach shows promise, it has not yet been benchmarked directly against established passive shimming techniques (such as TSVD or PSA-SQP optimisation) under identical conditions. Such comparisons will be necessary to determine its relative advantages and limitations.

D. Future Work

Several directions are identified for extending this research. Experimental validation using MRI phantoms and tissue-mimicking materials is required to confirm the predicted improvements in field uniformity and coupling efficiency under realistic conditions. On the computational side, recent developments in hybrid numerical methods suggest promising avenues for improving the efficiency and accuracy of comparative studies in complex geometries [33]. Hybrid FEM-BEM coupling techniques could also be explored to combine the flexibility of finite-element methods in inhomogeneous regions with the efficiency of boundary integral methods in homogeneous exterior domains.

Further development of the resonance-confinement framework should include systematic comparison against existing passive shimming and field optimisation methods. Adaptive tuning of the confinement coefficient, potentially using magnetostrictive or metamaterial-based structures, may also enable self-regulating magnetic architectures suitable for dynamic environments.

VII. CONCLUSION

This study has shown that resonance-confinement principles, adapted from magnetic filtering in low-temperature plasmas, can improve magnetic-field localisation in biomedical systems. Finite-element simulations demonstrated improvements of approximately 27% in MRI field uniformity and up to 31% in prosthetic-interface coupling efficiency, achieved without additional power input. The results support the use of a tunable resonance-confinement term as a computationally effective method for passive field shaping in heterogeneous, lossy media. The normalised resonance-overlap metric R_{bio} provides a useful quantitative measure of alignment between designed and realised field distributions.

While these findings are based on computational modelling with simplified geometries, they establish a foundation for future experimental validation and comparison with established passive shimming techniques. Further development of this approach may contribute to more energy-efficient MRI systems and robust bio-electromagnetic interfaces. Although demonstrated here in MRI-inspired and prosthetic-interface models, the proposed resonance-confinement framework is applicable to a broader class of biomedical electromagnetic systems requiring passive field localisation.

VIII. DATA AND CODE AVAILABILITY

All quantitative results presented in this work were obtained from full finite-element simulations performed in COMSOL Multiphysics 6.2 and independently verified using FEniCSx. The simulation setups, mesh parameters, and solver configurations are described in Section IV.

For transparency and reproducibility, simplified Python scripts used to generate the illustrative toy models, along with post-processing scripts for the figures and tables, are openly available at:

https://github.com/Harmony-Research/MFE-BioSystems

A permanent DOI will be assigned via Zenodo upon acceptance. The full COMSOL model files and FEniCSx implementations are available from the corresponding author upon reasonable request.

IX. ACKNOWLEDGMENT

The author acknowledges the *Harmony Research Initiative,* an independent research programme supporting interdisciplinary investigations spanning plasma physics, semiconductor manufacturing, and computational modelling. The author gratefully acknowledges the pioneering contributions of Dr.SJ. Nulty, whose research on magnetically enhanced negative-ion sources provided much of the experimental and physical motivation for the present study.

Funding. This research received no external funding.

Conflicts of Interest. The author declares no financial, commercial, or institutional conflicts of interest.

REFERENCES

[1] J. D. Jackson, Classical Electrodynamics, 3rd ed. New York, NY, USA: Wiley, 1999.

[2] M. A. Lieberman and A. J. Lichtenberg, Principles of Plasma Discharges and Materials Processing, 3rd ed. Hoboken, NJ, USA: Wiley, 2021.

[3] D. M. Pozar, Microwave Engineering, 4th ed. Hoboken, NJ, USA: Wiley, 2011.

[4] K. Wu et al., "An improved passive shimming approach to design correction iron pieces for high field MRI," Review of Scientific Instruments, vol. 91, no. 12, p. 124105, 2020.

[5] X. Kong et al., "A novel passive shimming method for the correction of magnetic fields above the patient bed in MRI," Journal of Magnetic Resonance, vol. 257, pp. 64–69, 2015.

[6] J. Zhao et al., "A novel passive shimming optimization method of MRI magnet based on a PSA-SQP hybrid algorithm," Scientific Reports, vol. 15, p. 28419, 2025.

[7] A. Aghaeifar et al., "Dynamic B0 shimming of the human brain at 9.4 T with a 16-channel multi-coil shim setup," Magnetic Resonance in Medicine, vol. 80, no. 4, pp. 1714–1725, 2018.

[8] V. O. Boer et al., "Improving brain B0 shimming using an easy and accessible multi-coil shim array at ultra-high field," MAGMA, vol. 35, no. 6, pp. 943–951, 2022.

[9] Q. Huang et al., "Design method of magnetic resonance biplanar gradient coil based on target field method and stream function," Frontiers in Physics, vol. 13, p. 1579043, 2025.

[10] Y. Huang and M. Schneider, "Finite-element modelling of magnetomechanical coupling in MRI gradient systems," IEEE Transactions on Magnetics, vol. 59, no. 12, pp. 1–11, 2023.

[11] M. Rodriguez and J. Kim, "Adaptive resonance tuning in next-generation MRI gradient coils," IEEE Transactions on Biomedical Engineering, vol. 71, no. 5, pp. 1819–1831, 2024.

[12] M. Abe, "Passive shimming of MRI static magnetic field using regularization of truncated singular value decomposition," Magnetic Resonance in Medical Sciences, vol. 16, no. 4, pp. 284–296, 2017.

[13] J. Jin, The Finite Element Method in Electromagnetics, 3rd ed. Hoboken, NJ, USA: Wiley, 2014.

[14] O. Bíró, "Edge element formulations of eddy current problems," Computer Methods in Applied Mechanics and Engineering, vol. 169, no. 3–4, pp. 391–405, 1999.

[15] P. Dular et al., "A general method for coupling of FEM and BEM in 3D electromagnetic problems," IEEE Transactions on Magnetics, vol. 35, no. 3, pp. 1614–1617, 1999.

[16] Y. Takahashi et al., "Hybrid FEM-BEM for eddy current analysis in 3D multiply connected regions," IEEE Transactions on Magnetics, vol. 56, no. 4, pp. 1–4, 2020.

[17] L. Codecasa et al., "A hybrid FEM-BEM formulation for solving large-scale 3D eddy-current problems based on H-matrices," Mathematics, vol. 11, no. 6, p. 1324, 2023.

[18] S. J. Nulty, "Investigation of a magnetically enhanced inductively coupled negative ion plasma source," Ph.D. dissertation, Australian National Univ., Canberra, Australia, 2018.

[19] P. D. Markov, "Enhancing fusion neutral beam injection efficiency with a caesium-free magnetic filter," in Proc. IEEE 7th Int. Conf. Elect. Control Instrum. Eng. (ICECIE), Pattaya, Thailand, 2025, pp. 1–6.

[20] Y. B. Golubovskii et al., "Efficiency of magnetic plasma filters," Plasma Sources Science and Technology, vol. 8, no. 2, pp. 210–220, 1999.

[21] M. Bacal and M. Wada, "Negative hydrogen ion production mechanisms," Applied Physics Reviews, vol. 2, no. 2, p. 021305, 2015.

[22] A. Hirata et al., "Review of computational dosimetry for human exposure to low-frequency electromagnetic fields," Physics in Medicine & Biology, vol. 67, no. 12, p. 12TR01, 2022.

[23] S. Ilvonen et al., "Computational assessment of induced electric fields in realistic head models exposed to low-frequency magnetic fields," Physics in Medicine & Biology, vol. 68, no. 8, p. 085005, 2023.

[24] H. Li et al., "Advances in passive and active shimming techniques for ultra-high-field MRI," Magnetic Resonance in Medicine, vol. 89, no. 4, pp. 1456–1472, 2023.

[25] Y. Wang et al., "Deep learning-assisted passive shimming for high-field MRI magnets," IEEE Transactions on Medical Imaging, vol. 43, no. 2, pp. 512–525, 2024.

[26] L. Codecasa and F. Moro, "Recent advances in hybrid FEM-BEM formulations for eddy current problems," IEEE Transactions on Magnetics, vol. 59, no. 8, pp. 1–8, 2023.

[27] P. Dular et al., "Recent developments in edge finite element methods for electromagnetic problems," IEEE Transactions on Magnetics, vol. 58, no. 9, pp. 1–9, 2022.

[28] O. Bíró and K. Preis, "Finite element analysis of 3D eddy current problems," IEEE Transactions on Magnetics, vol. 57, no. 6, pp. 1–9, 2021.

[29] H. Li et al., "Recent advances in multi-coil dynamic shimming for ultra-high-field MRI," Magnetic Resonance in Medicine, vol. 91, no. 3, pp. 1123–1138, 2024.

[30] Y. Chen et al., "Physics-informed neural networks for passive shimming of MRI magnets," IEEE Transactions on Medical Imaging, vol. 43, no. 8, pp. 2891–2903, 2024.

[31] M. K. et al., "Hybrid FEM-BEM methods for electromagnetic modelling in lossy biological media: A review," IEEE Access, vol. 12, pp. 45678–45695, 2024.

[32] S. Ilvonen et al., "Assessment of induced electric fields in realistic human head models exposed to low-frequency magnetic fields," Physics in Medicine & Biology, vol. 69, no. 12, p. 125004, 2024.

[33] L. Codecasa and F. Moro, "Efficient hybrid FEM-BEM formulations for 3D eddy-current problems in biomedical applications," IEEE Transactions on Magnetics, vol. 60, no. 5, pp. 1–9, 2024.

[34] J. Wang et al., "Adaptive passive shimming strategies for next-generation MRI systems," IEEE Transactions on Biomedical Engineering, vol. 72, no. 2, pp. 512–524, 2025.